

Barycentric convolution surfaces based on general planar polygon skeletons

Xiaoqiang Zhu^a, Chenze Song^a, Mengyao Zhu^a, Xiangyang Wang^a, Lihua You^b, Xiaogang Jin^c

^a School of Communication and Information Engineering, Shanghai University, Shanghai 200444, China

^b National Center for Computer Animation, Bournemouth University, Poole, BH12 5BB, UK

^c State Key Lab of CAD&CG, Zhejiang University, Hangzhou 310058, China

ARTICLE INFO

Keywords:

Convolution surfaces
Polygon skeleton
Barycentric coordinates
Support radius

ABSTRACT

Using barycentric coordinates for thickness interpolation, we present a novel polygonal skeleton based convolution surface approximation method with varying radii. Given the prescribed radii of an arbitrary planar polygonal skeleton, we first employ a smooth interior mean value coordinate interpolation approach to calculate the thickness at each projection position in the polygonal plane. Then a local thickness approximation method based on finite support kernels is introduced to create an implicit surface with smoothly varying thickness. In addition, a polygon offset with different distances by winding numbers is employed to create local approximation at polygon boundaries. Our experiments show that the proposed uniform smooth thickness interpolation and local convolution approximation method can not only avoid surface wrinkles but also reduce computation cost. Moreover, our approach is insensitive to exterior thickness interpolation. Therefore smooth barycentric coordinates within a polygon can all be easily integrated into our approach.

1. Introduction

Efficient skeleton-driven 3D modelling is commonly applied in both explicit surfaces [1] and implicit surfaces [2]. As one of the most important implicit surfaces, a convolution surface is defined by convolving a skeleton with a three-dimensional, low pass filter kernel [3], and it provides a powerful means to design smooth branching shapes through intuitive skeletons [4]. The superposition and smoothness properties enable its well-behaved blending with underlying skeletons. Using convolution surfaces, users can design a complex smooth shape by assembling different parts controlled by underlying skeletons [5]. Because of its integral form, much attention has been given to design efficient closed-form solutions to reduce the computation cost. According to the mathematical formulations of convolution surfaces, we observe that there are limited choices of kernel functions and skeletal primitives that can be convolved together analytically. Although there are some analytical solutions for one-dimensional skeletons (e.g. lines, arcs and quadratic curves) with a varying kernel [4,6–8], the solutions for two-dimensional skeletons with varying radii are still not well investigated. Such a solution is quite useful for creating more complex polygon skeleton-based convolution shapes with varying thickness.

Recently, convolution surfaces have also been successfully employed in the Brush2Model system [9] which allows users to create smooth shapes by sketching 3D skeletons in a HMD environment. Although the analytical convolution approximation for skeleton models with a user-

defined radius is proposed in their approach, polygonal skeletons have to be triangulated and subdivided for surface design as no closed-form solutions can be directly derived for varying radii at polygon vertices. Similarly, inspired by convolution surfaces, SCALE-invariant Integral Surfaces (SCALIS) [10] are designed for radius control in which the radius of the surfaces around a skeleton can be explicitly controlled. The generated blending shapes are self-similar regardless of the scale of the model. However, the linearly varying thickness control based on polygonal skeletons has to be performed using numerical integration.

In this paper, we present a novel convolution surface modelling approach to create 3D sheet-like shapes with smoothly varying thickness based on a polygonal skeleton, which is important in an interactive modelling system. In order to create shapes allowing not only local radius adjustment but also global smoothness, analytical solutions for mean value coordinates are derived to model smoothly varying thickness at any point on an arbitrary polygon. Moreover, the barycentric thickness is introduced to derive a closed-form local convolution surface approximation based on a polyline or a polygonal skeleton.

The remainder of the paper is organized as follows. After introducing the related work in Section 2, convolution surfaces with finite support are described in Section 3. Then we give a brief definition of barycentric coordinates and the chosen mean value coordinates for our applications in Section 4. In Section 5, the convolution surface approximation based on mean value coordinates is derived, followed by the implementation details and some modelling results with our approach in Section 6, and our paper ends with the conclusion given in Section 7.

2. Related work

Although quite a lot of works are related to our approach, the most relevant ones include convolution surfaces and barycentric coordinates, which will be detailed below.

Convolution surfaces were first proposed by Bloomenthal and Shoemake [3] to create smooth surfaces by convolving geometric skeletons with a Gaussian kernel function. To avoid the global support of such kernels as Gaussian function and Cauchy function, finite supported ones [4,11] are usually preferred due to their locality property. As the high computation costs of convolution integration hinders its use, derived closed-form solutions [12] make it feasible for convolution surfaces to be employed in many interactive systems [5,9,13]. In theory, any geometric models can serve as convolving skeletons, while line segments [14,15] are the most commonly used to generate cylindrical or branching rounded shapes, and anisotropic convolution surfaces [16,17] generated from 1D line skeletons are proposed to increase modelling freedom. If a planar surface is required, using polygonal skeletons is the most suitable option, in the case where their solutions can be analytically represented [5,18,19]. In order to obtain as rich shapes as possible, the varying radii along 1D line skeletons facilitate smooth manifold surfaces with varying thickness [6–8]. Recently, scale-invariant integral surfaces built on convolution surfaces have been proposed [10], which can also approximate the prescribed radii at line segment vertices. To the best of our knowledge, however, no analytical solution exists for convolving polygonal skeletons with varying weights, which is frequently computed by a multi-level polygon subdivision and a subsequent uniform-radius polygon convolution. Although Zanni proposed a semi-numerical integration approach [2] with a limited level of adaptivity, it is not general for arbitrary polygons. Based on the implicit relations between the thickness of convolution surfaces and the support radii of the embedded skeletons [9], a barycentric policy is employed to generate convolution surfaces with smoothly varying thickness. In addition, convolution has been recently employed to model excellent heterogeneous objects [20] and generate smooth distance functions [21] with high-quality continuity.

Barycentric coordinates include Wachspress coordinates [22], Harmonic coordinates [23], Mean value coordinates [24–26], Green coordinates [27,28], Poisson coordinates [29] and so on, which are usually used to create cage-based coordinates for linear data interpolation. Actually due to many optimal properties such as smoothness, linear reproduction, Lagrange property, partition of unity and non-negativity, they are commonly used in 2D/3D shape deformation [28,30–32]. In this paper, mean value coordinates which achieve all the above-mentioned advantages will be used for our formulation. If local control is required, an umbrella shaped cell [28], local barycentric coordinates [33], subdividing barycentric coordinates [34] or blended barycentric coordinates [35] can be utilized. In the recent work [36], cubic mean value coordinates for interpolating Hermite constraints were proposed which recently were further simplified and efficiently implemented in [37].

3. Convolution surfaces with finite support kernel

A convolution surface is an iso-surface embedded in a 3D field generated by convolving a kernel function with a geometric skeleton. Given a geometric skeleton:

$$g(\mathbf{p}) = \begin{cases} 1, & \mathbf{p} \in \text{skeleton} \\ 0, & \text{otherwise} \end{cases} \quad (1)$$

and a kernel function $f: R^3 \rightarrow R$, the accumulated field at \mathbf{p} is the convolution integral of the functions g and f :

$$F(\mathbf{p}) = \int_V g(\mathbf{q})f(\mathbf{p}-\mathbf{q})dV = (f \otimes g)(\mathbf{p}). \quad (2)$$

In theory, any low-pass filtering kernels and geometric skeletons can be paired to define a convolution scalar field, but elaborate strategies are needed if an efficient computation is expected. Here two aspects are

taken into account. Firstly, a polynomial kernel with closed-form solutions is preferred due to its lower computation cost compared to other exponential ones. Secondly, a local support kernel will cut off skeleton segments which are too far away from the current position in question. Owing to the above reasons, a finitely supported quartic kernel

$$f_{\text{quartic}}(r) = \begin{cases} \left(1 - \frac{r^2}{R^2}\right)^2, & r \leq R \\ 0, & r > R \end{cases} \quad (3)$$

is employed in our approach, where R is the skeleton's support radius. Thus only the clipped part of a skeleton is convolved, which reduces the computational cost.

4. Barycentric coordinates for an arbitrary planar polygon

For a planar polygon P with n vertices v_i ($i = 1, 2, \dots, n$) $\in R^2$, the functions $w = [w^1, w^2, \dots, w^n]: P \rightarrow R^n$ are called generalized barycentric coordinates if the following properties are satisfied:

- 1) Partition of unity property: $\sum_{i=1}^n w_i(x) = 1 \quad \forall x \in P$;
- 2) Reproduction property: $\sum_{i=1}^n w_i(x)v_i = x \quad \forall x \in P$;
- 3) Lagrange property: $w_i(v_j) = \delta_{ij} = \begin{cases} 0, & \text{if } i \neq j \\ 1, & \text{if } i = j \end{cases}, i, j = 1, \dots, n$, where δ_{ij} is the Kronecker delta;
- 4) Linearity: the functions w_i are linear on polygon edges;
- 5) Smoothness: the functions w_i vary smoothly on P ;
- 6) Locality: each vertex of P only influences its nearby regions, and a point $x \in P$ is influenced by a small number of the vertices of P ;
- 7) Non-negativity: $w_i \geq 0 \quad \forall i$.

Theoretically, a unique solution $w_i(x)$ ($i = 1, 2, 3$) can be found for a triangle. However, various solutions may exist for a n -sided ($n > 3$) polygon. Rational functions based Wachspress coordinates have such advantages as non-square roots, easy evaluation and simple upper bounds on the gradients, and they can be applied to any convex polygons. However, for star-shaped polygons and arbitrary polygons, Wachspress coordinates are not well-defined, which means they are limited to convex polygons since the denominator in the rational expression becomes zero at certain points in the concave polygon. Therefore optimal GBC (General Barycentric Coordinates) should be chosen for our convolution surface approximation based on arbitrary planar polygon skeletons.

As one of the most popular kind of GBC [25], mean value coordinates (MVC) can be defined as:

$$w_i(x) = \frac{\tan(\alpha_{i-1}/2) + \tan(\alpha_i/2)}{|v_i - x|}, \quad (4)$$

with the angles $0 < \alpha_j = \alpha_j(x) < \pi$, as shown in Fig. 1. Although mean value coordinates are no longer positive if the polygon is not star-shaped, they are very general and surprisingly robust over complex geometric shapes, provided that the angles α_i are treated as signed angles. That is, if the unit vector $e_i := (v_i - x)/|v_i - x| = (\cos \theta_i, \sin \theta_i)$, then

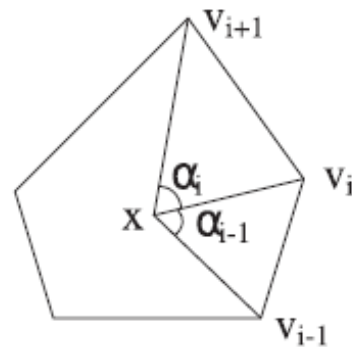


Fig. 1. Notation for mean value coordinate.

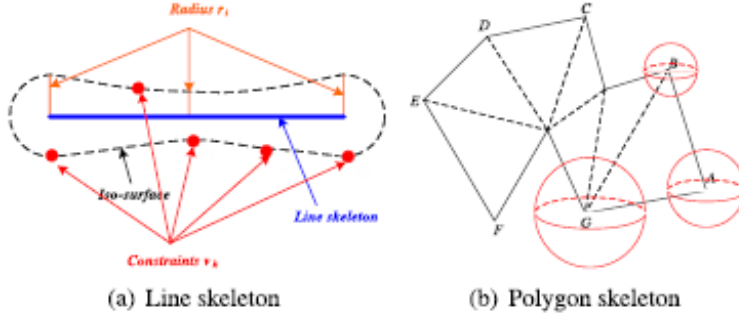


Fig. 2. Non-uniform skeletal weight distribution.

$\alpha_i = \theta_{i+1} - \theta_i$ has the same sign as $\epsilon_i \times \epsilon_{i+1}$. The reason for MVC's robustness is that even though each $w_i(x)$ in Eq. (4) could not be guaranteed to be positive for arbitrary P , the sum $\sum_{i=1}^n w_i(x)$ is always positive for any x in P . The details can be referenced in [25], where more good properties such as the Lagrange and piece-wise linearity properties on ∂P can also be found. Furthermore, closed-form solutions for MVC coordinates are defined all over the whole polygonal plane which is useful for our convolution interpolation as the potential field computation outside the polygonal skeleton has to be performed for iso-surface extraction. Due to these nice properties of MVC, we will employ it in our polygon thickness interpolation and convolution surface approximation. Moreover, we can utilize the blended barycentric coordinates [35] based on MVC to further extend our approximation for locality property.

5. Barycentric approximation with convolution surfaces

Although a convolution surface is usually not a preferred tool to interpolate complex shapes with very high precision, its embedded skeletons allow to efficiently edit the model interactively. Thus an intuitive and sufficiently accurate fitting approach is essential to create a convolution surface with the prescribed thickness at different positions of the skeleton.

5.1. General line skeleton interpolation

As illustrated in Fig. 2(a), by adjusting the support radii of a polyline segment, a cylinder/prism-like convolution surface with varying thickness is preferred to encapsulate the embedded skeleton. For a series of skeletons, the total convolved field creates a blended iso-surface which can be defined as:

$$S = \left\{ p \mid \sum_{i=1}^n \lambda_i f_i(p) - T = 0 \right\}, \quad (5)$$

where f_i and λ_i are the field and contribution weight of each skeleton, and T is the threshold of the iso-surface.

As discussed in [15], although a global NNLS (Non-Negative Least Squares) is a reasonable method to fit the skeletons with assigned radii by applying some constraint vertices, bulging artifacts will arise because of noises or constraint distributions. Therefore, a better solution using local thickness approximation is employed here to generate more pleasing shapes, based on the assumption that the embedded skeleton segment is long enough. A similar idea was also proposed by Zanni et al. in [10]. If a line skeleton with uniform support radius R_i is used to approximate the desired thickness d of the convolution surface, the local weight λ_i of the current skeleton can be derived as [15]:

$$\begin{aligned} F(p) &= 2\lambda_i \int_0^{\sqrt{R_i^2 - d^2}} \left(1 - \frac{d^2 + x^2}{R_i^2} \right)^2 dx = T, \\ \Rightarrow \lambda_i &= \frac{15TR_i^4}{16(R_i^2 - d^2)^{\frac{5}{2}}}. \end{aligned} \quad (6)$$

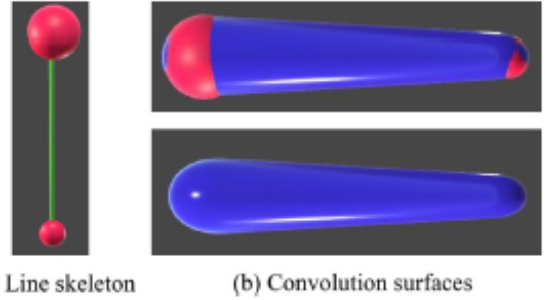


Fig. 3. Line skeleton based convolution surfaces.

To design a convolution surface, the preferred support radius is usually set as $R_i = 2d$ and its weight is set to $\lambda_i = \frac{15\sqrt{3}T}{9R_i}$.

Based on the local approximation of a line skeleton with a uniform radius [15], here we generalize it to varying radii along a line segment. For a line segment with radii r_i at its vertices v_i ($i = 1, 2$) and under the assumption that the projection v_1v_2 of an arbitrary 3D position p is $p' = uv_1 + (1-u)v_2$, the field contribution at p should be set as $\lambda_p = u\lambda_1 + (1-u)\lambda_2$ using a uniform support radius $r = \max(r_1, r_2)$. Since a uniform support radius leads to inferior approximation especially at thin/thick parts with large/small radii, a better solution in practice is to interpolate the support radius at projection p' : $R = uR_1 + (1-u)R_2$, which is then employed to compute the contribution weight with Eq. (6) (Fig. 3). It is coincident that, if λ_i in Eq. (6) is moved inside the integral, then the formulation is strictly equivalent with the one of [10].

5.2. Arbitrary polygon skeleton interpolation

Although a similar scheme can also be applied to polygonal skeletons (Fig. 2(b)), the barycentric coordinate of an arbitrary 2D projection in a planar polygon is not unique anymore except for a triangle. As our barycentric convolution surfaces with varying thickness depend on the definition of barycentric coordinates, global barycentric coordinates will bring smooth convolution surfaces without unnatural transitional regions near in-between boundaries of sub-polygons. That is, for a globally smooth convolution surface based on a polygon with varying thickness, the thickness interpolations at different positions should be independent of different groups of vertices in order to generate artifacts free surfaces between regions of different groups. What we need is a relatively large planar polygon, thus a smooth enough interpolation for arbitrary planar polygons is essential here. The reason for this is that a unique interpolation solution for triangulated polygon (Fig. 4(a)) results in obvious C^0 -continuity at joints between neighboring sub-triangles (Fig. 4(c)), as interpolation along interior triangulated edges is linear according to the linearity property 4) of general barycentric coordinates. Fortunately, the barycentric coordinate interpolation for the

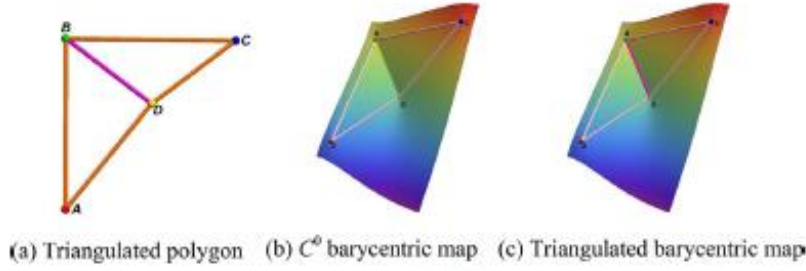


Fig. 4. Barycentric weighted height map interpolation for 4-sided concave polygon.

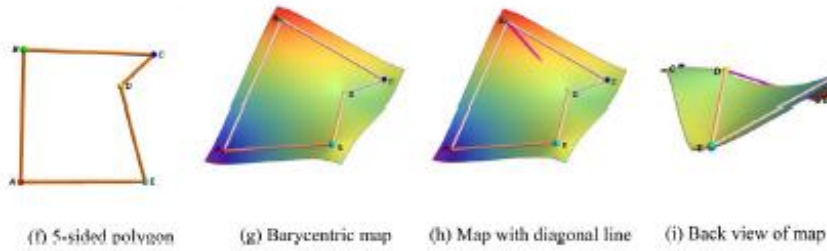
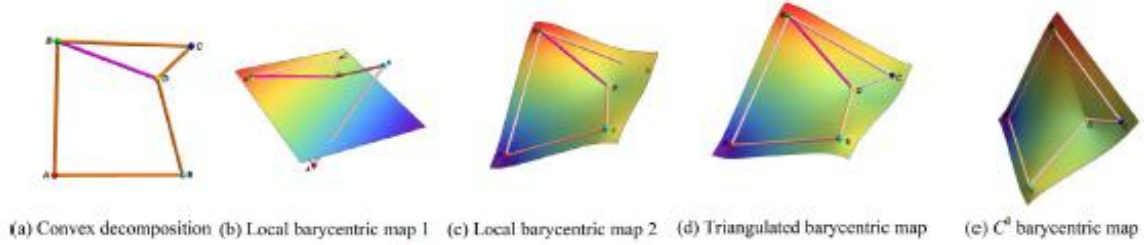
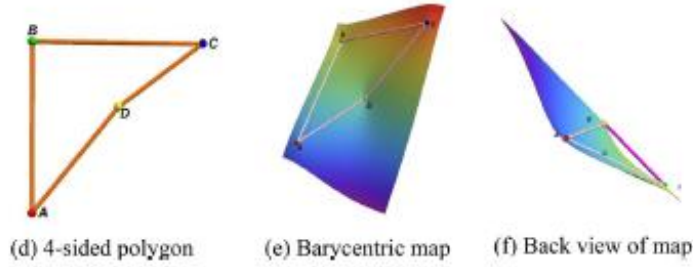


Fig. 5. Barycentric weighted height map interpolation for 5-sided concave polygon.

entire polygon (Fig. 4(d)) produces smooth results everywhere (Fig. 4(e)) except at the vertices, even though no exact interpolation along diagonals (Fig. 4(f)) can be created. In fact, a polygon with more vertices will lead to more serious problems if a triangulation policy is involved (Fig. 5). When a 5-sided polygon ABCDE is subdivided into a triangle BDC and a quadrilateral AEDB (Fig. 5(a)), single barycentric interpolation for BDC or AEDB does not pass through the other vertices of ABCDE (Fig. 5(b), (c)). If both of the two subdivided polygons are used to interpolate the vertices at the same time (Fig. 5(d)), obvious C^0 -continuity occurs between them (Fig. 5(e)). Therefore a uniform barycentric interpolation achieves expected smoothness, vertex interpolation and linearity property along polygon boundaries. More practical experiments validating general barycentric interpolation for convolution surface approximation will be detailed in the next section.

Unlike line skeletal approximation, a polygonal skeleton-based convolution surface involves 2D integral calculation. If the v_i ($i = 1, 2, \dots, n$) of a n -sided planar polygon are assigned thickness r_i ($i = 1, 2, \dots, n$), the anticipated radius of an arbitrary 2D projection p' can be

computed as:

$$r(p') = \sum_{i=1}^n w_i(p') \cdot r_i, \quad (7)$$

where w_i is the barycentric (here mean value coordinates are used) coordinates of the polygon, where Eq. (4) can be directly applied. Then a local approximation similar to [38] and [9] is employed based on the assumption that the convolving planar polygon is large enough. After that, a preferred twice-support radius $R_{sp} = 2 \cdot r(p')$ is used to derive a local convolution approximation:

$$F(p) = 2\lambda \int_0^{2\pi} \int_0^{\sqrt{R_{sp}^2 - r^2}} \left(1 - \frac{r^2(p') + r^2}{R_{sp}^2}\right)^2 r dr d\theta = T, \\ \Rightarrow \lambda = \frac{3R_{sp}^4 T}{\pi(R_{sp}^2 - r^2(p'))^3} = \frac{64T}{9\pi R_{sp}^2}. \quad (8)$$

As λ is inversely proportional to R_{sp}^2 , Eq. (8) can also be regarded as another 2D version of the equation in [10]

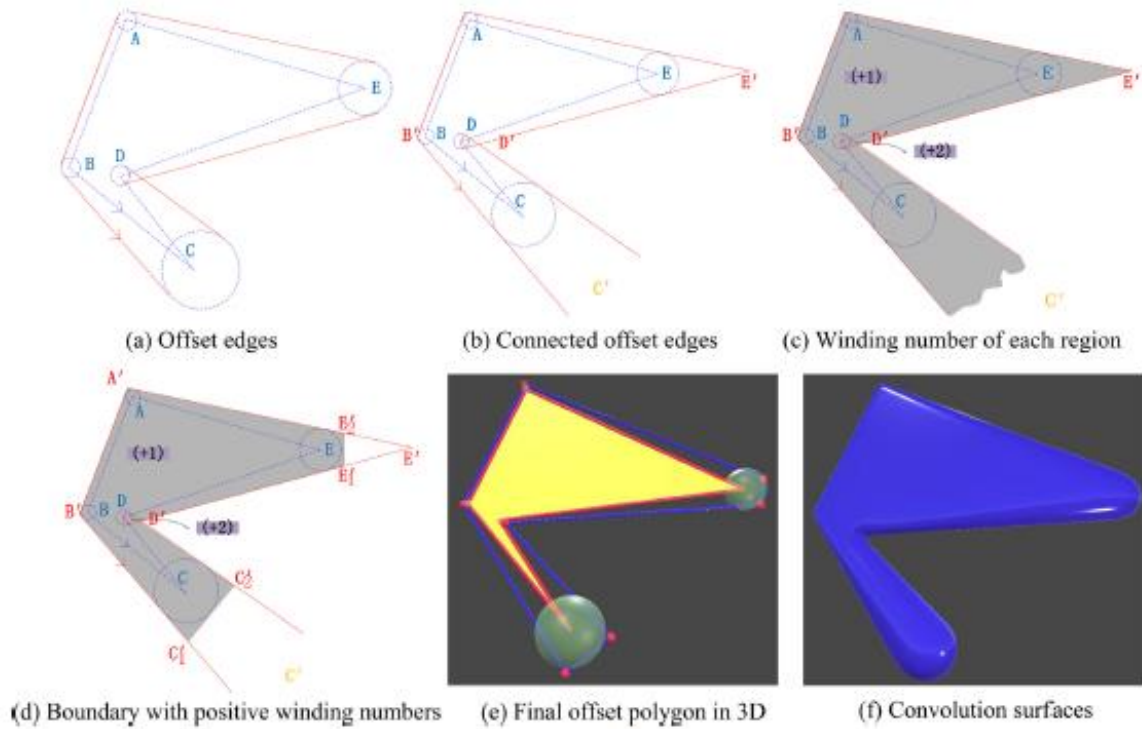


Fig. 6. Winding number external offset with varying radii.

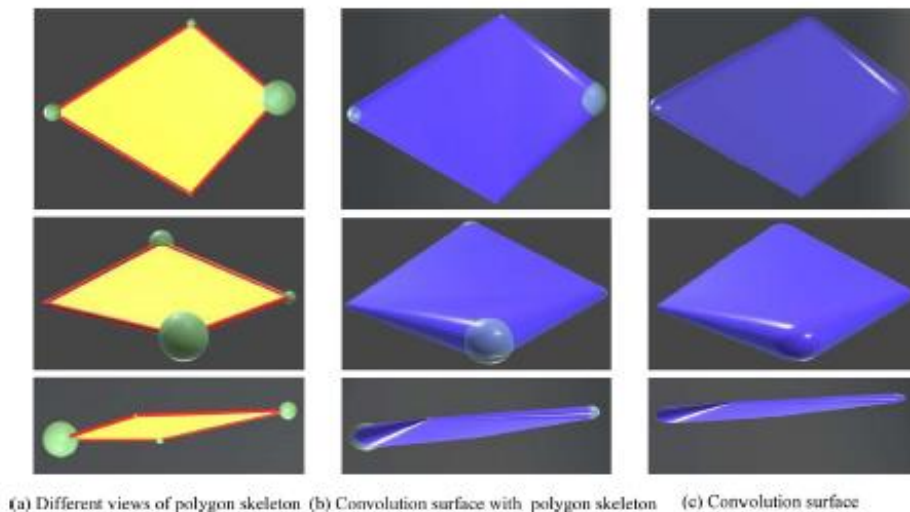


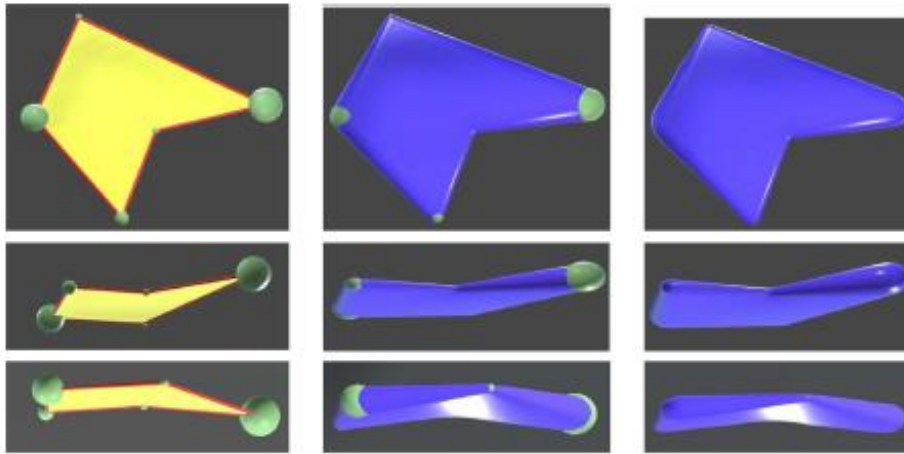
Fig. 7. Convolution surface based on 4-sided convex polygon skeleton.

5.3. Polygon offset extension

Due to the shrinkage problem of convolution surface approximation at boundaries, extended line segments or polygons are used to compensate the undesirable effects [9,10]. For a polygon skeleton, an image-space-based inflation is employed in [9]. Unfortunately too many vertices on the inflated contour have to be extracted in their approach, which is not efficient for our subsequent barycentric interpolation. According to the conclusion of Eq. (14) in [9] ($u = 0.42428R_{sp}$, where u is

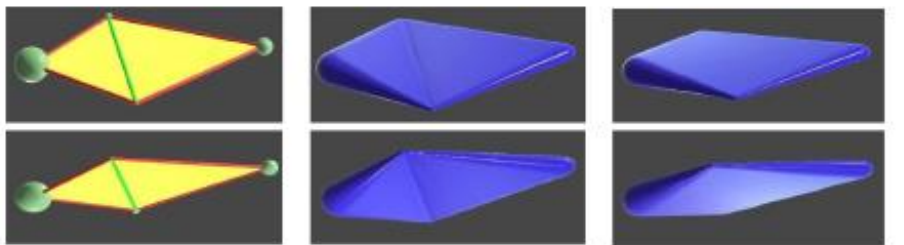
the offset distance), the offset distance at a separate vertex of a polygon was proportional to its local support radius. Therefore, a revised winding number external offset algorithm [39] with varying offset distances is utilized for creating a larger skeleton (Figs. 6–7) which consists of the following steps.

Step 1. According to the direction of the edges of the directional polygon, the edges are offset to the right side by the anticlockwise rule (Fig. 6(a)).



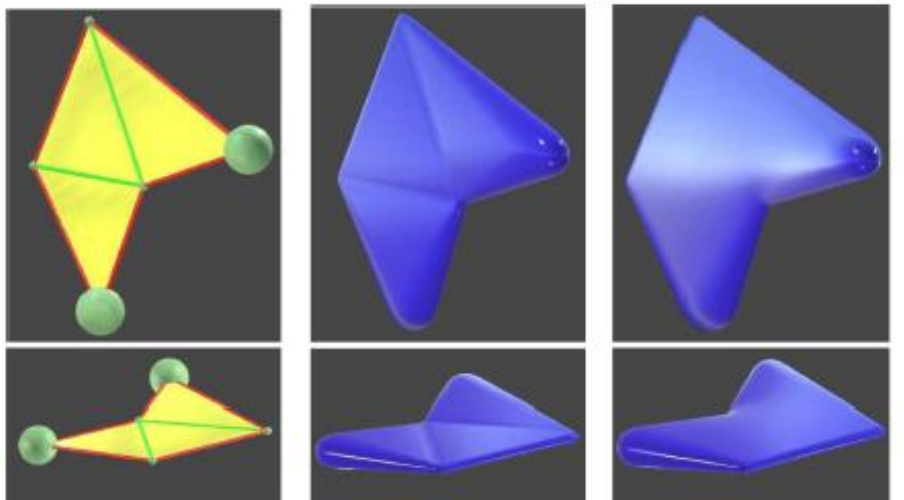
(a) Different views of polygon skeleton (b) Convolution surface with polygon skeleton (c) Convolution surface

Fig. 8. Convolution surface based on 5-sided concave polygon skeleton.



(a) Different views of polygon skeleton (b) Convolution surface based on sub-skeletons (c) Convolution surface based on the unified skeleton

Fig. 9. Comparison between convolution surfaces based on 4-sided convex polygon skeleton.



(a) Different views of polygon skeleton (b) Convolution surface based on sub-skeletons (c) Convolution surface based on the unified skeleton

Fig. 10. Comparison between convolution surfaces based on 5-sided concave polygon skeleton.

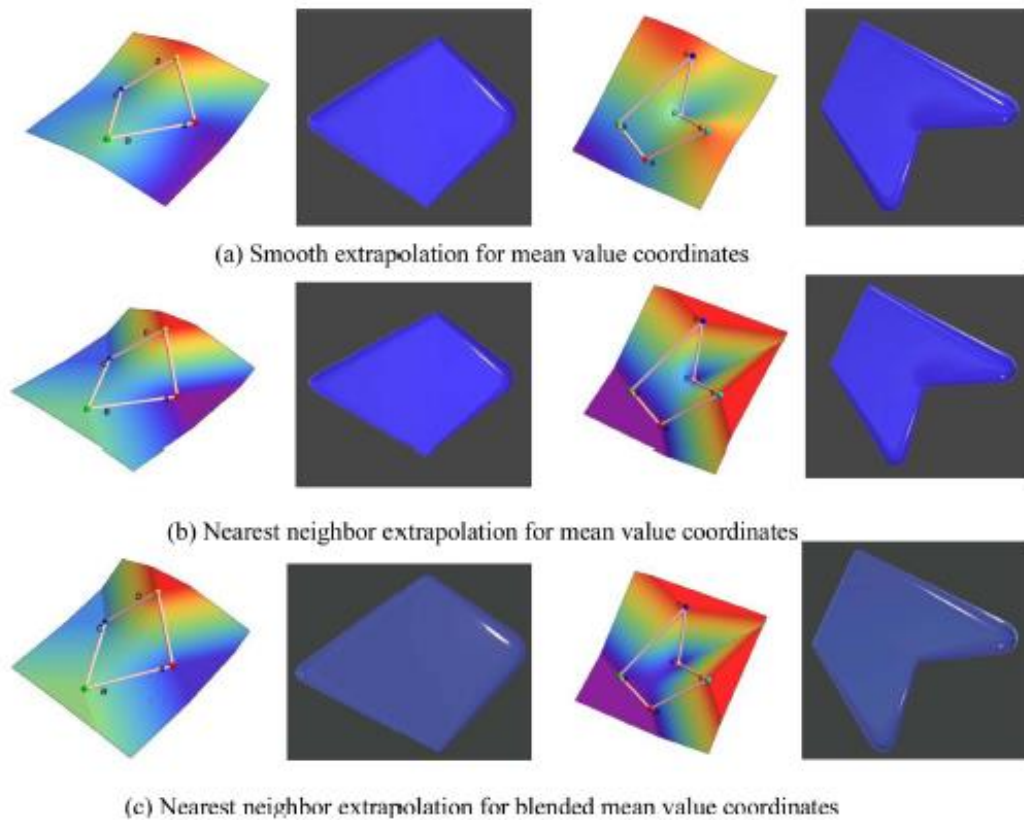


Fig. 11. Different extrapolations for different mean value coordinates.

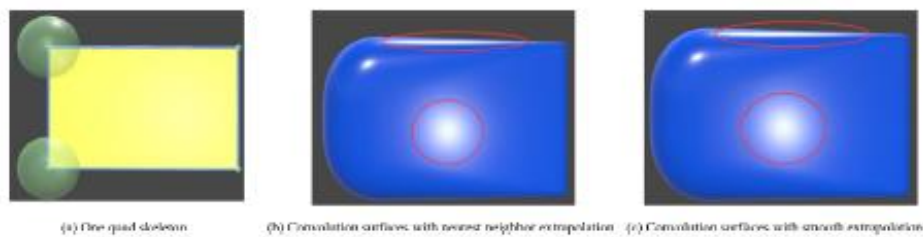


Fig. 12. Convolution surfaces based on one quad skeleton.

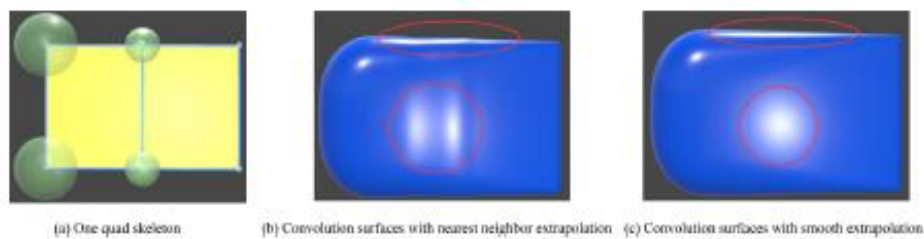


Fig. 13. Convolution surfaces based on two connected quad skeletons.

Step 2. As shown in Fig. 6(b), if the vertex is a convex vertex, the end vertices of the offset edge are extended and intersected. If the vertex is a concave vertex, the endpoints of the offset segment are connected to the current vertex with a straight line segment.

Step 3. The zones with positive winding numbers relative to the offset curve are categorized as being inside the offset poly-

gon and their joint boundary is the final outer offset polygon (Fig. 6(c)).

As the offset distance changes along the edge with different radii, convex vertices may produce non-intersected extended offset lines or the intersection is too far away from the current vertex, such as the vertices C and E in Fig. 6(c)-(e). A mitered offset solution can solve the

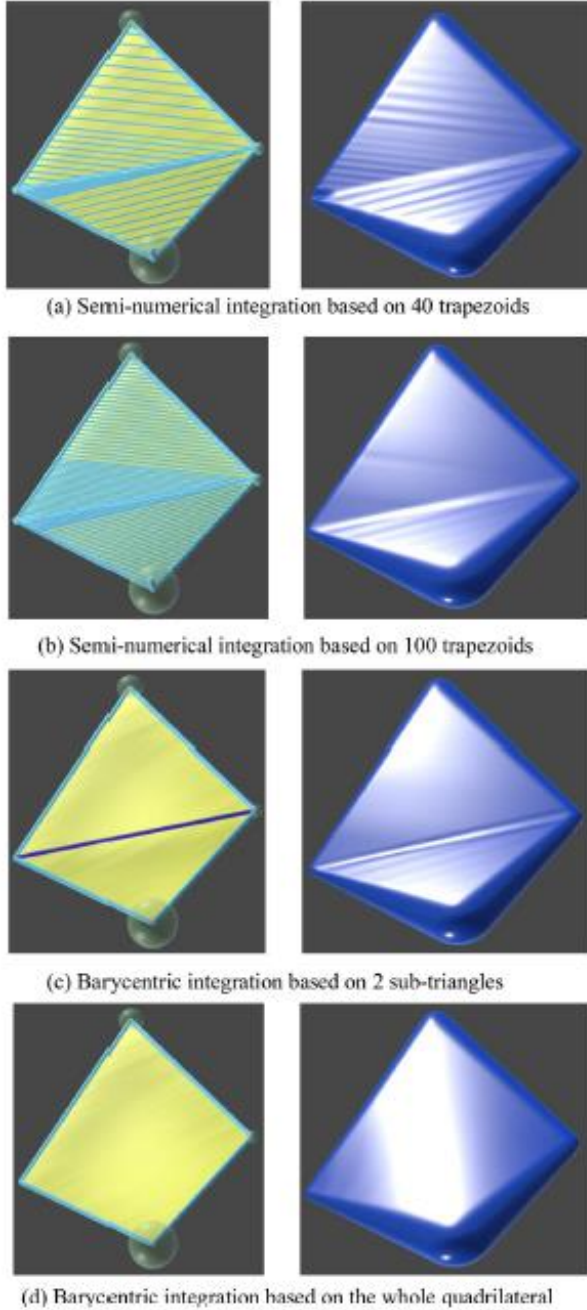


Fig. 14. Different integration policies for a 4-sided polygon.

problem when the distance d between the intersection C/E and the original vertex C/E is greater than a threshold $d_{threshold} = 2R$, where R is the support radius of the current convex vertex, as only the skeletons within the support sphere have convolution field contributions. As a matter of fact, the offset policy can also be applied to SCALIS surfaces [10] provided that the polygon skeletons are tessellated into triangles.

6. Experiments and results

To demonstrate the efficiency of the proposed barycentric interpolation of a polygonal skeleton-based convolution surface, several convolution surface models based on polygonal skeletons with varying radii are created in our experiment on a PC with a 4.0 GHz Intel Core i7-6700K CPU (only 1 core is used) with 16 GB memory. Both the convolution potential fields and the iso-surface extraction ($200 \times 200 \times 200$ Marching Cubes) are performed in the Unity3D engine and core calculation steps are implemented with C# language on CPU, which could be accelerated using parallel computation on GPU.

Figs. 7 and 8 show convolution surfaces based on a convex 4-sided and a concave 5-sided planar polygon, which achieves smoothly varying thickness. It can be seen that our approach can deal with both convex and concave polygons and approximate the anticipated skeleton shapes well. Although a triangulation-based approach can produce similar shapes, obvious seams arise between neighboring sub-triangles (Figs. 9(b), 10(b)), which can be avoided by our unified polygonal barycentric interpolation (Figs. 9(c), 10(c)). Therefore, when a concave polygon skeleton is involved, decomposing it into convex parts before barycentric interpolation and convolution field calculation is not preferred, especially when the radii at vertices vary too rapidly. The seams in Figs. 9 and 10 are due to the discontinuous interpolation between sub-triangles, which results from the fact that regions near the in-between boundary of sub-triangles are interpolated using distinct groups of vertices.

In addition, the barycentric interpolation for polygon skeleton-based convolution surfaces is robust regardless of different external barycentric interpolations if only one skeleton is involved without further blending operations. Fig. 11(a) presents regular mean value coordinate interpolation both inside and outside of the polygon, a very smooth weight map interpolation is created and it can be adopted to produce pleasing convolution surfaces. It is worth mentioning that, if a regular mean value coordinate interpolation only applies to the inside of the polygon and the outside interpolation is replaced by its nearest position of the polygon, very similar results can also be achieved (Fig. 11(b)). The reason is that, the nearest neighbor extrapolation method generates piecewise constant weights, which does not vary too rapidly. This implies that all other general barycentric coordinates can also be employed in our framework, even though their interpolations for the outside of a planar polygon are not well-defined, such as the blended barycentric coordinates [35] (Fig. 11(c)).

However, there is still discrepancy between the smooth extrapolation and the nearest neighbor extrapolation methods. For comparison, a quad skeleton with coordinates and linear weights of $((0, 0, w = 0.5), (0, 1, w = 0.5), (1.5, 0, w = 0.05), (1.5, 1, w = 0.05))$ is designed in Fig. 12(a). We can find that there is no visible difference between the produced convolution surfaces with the nearest neighbor extrapolation (Fig. 12(b)) and the smooth extrapolation policies (Fig. 12(c)). In Fig. 13(a), the QUAD is divided into two connected quad skeletons with the coordinates and weights as: QUAD1 $((0, 0, w = 0.5), (0, 1, w = 0.5), (0.75, 0, w = 0.275), (0.75, 1, w = 0.275))$, QUAD2 $((0.75, 0, w = 0.275), (0.75, 1, w = 0.275), (1.5, 0, w = 0.05), (1.5, 1, w = 0.05))$. Visible bulges arise in the connection region when a nearest neighbor extrapolation approach is employed (Fig. 13(b)), while the same surface as one whole quad skeleton (Fig. 12(c)) can be created using smooth extrapolation (Fig. 13(c)). Therefore, the smooth extrapolation method keeps the superposition property of convolution surfaces, while the nearest neighbor extrapolation does not. The seam artifacts in Figs. 9 and 10 are due to the non-continuous interpolation across the boundary line between sub-polygons, and it does not contradict with the superposition property of convolution surfaces. That is to say, the thickness at some place within the polygon plane should depend on all or most of the polygon vertices rather than only a small part of them.

Table 1

Comparison between convolution surfaces based on weight/support radius interpolation.

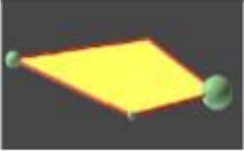
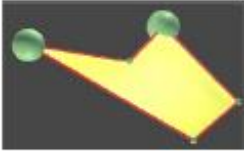
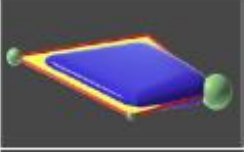
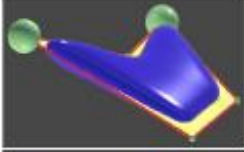
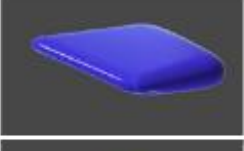
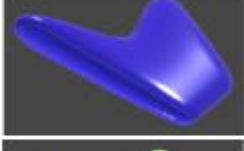
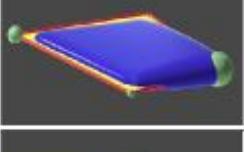
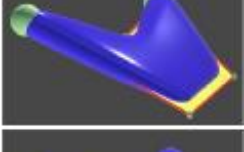
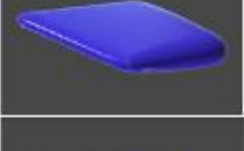
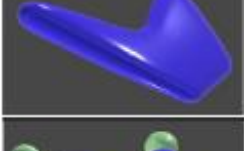
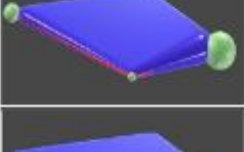
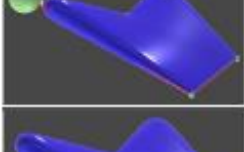
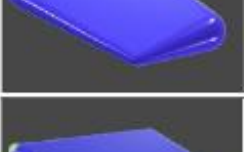
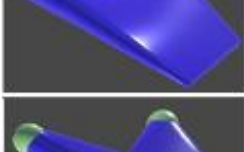
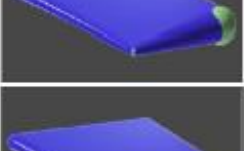

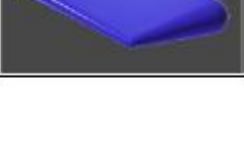

Polygon skeleton		(a)		
Field weight interpolation	Based on original skeleton	(b)		
		(c)		
	Based on offset skeleton	(d)		
		(e)		
		(f)		
Support radius interpolation	Based on original skeleton	(g)		
		(h)		
	Based on offset skeleton	(i)		

Table 2
Comparison between triangulation scheme and our barycentric approach.

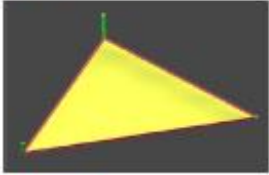
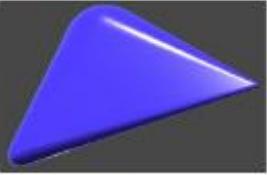
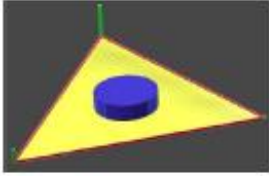
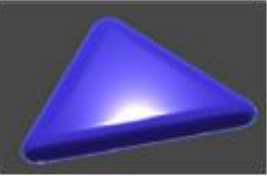
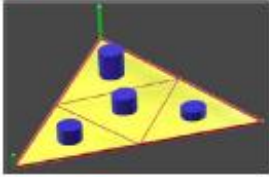
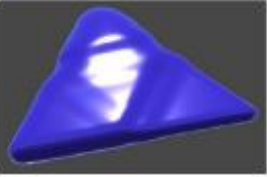
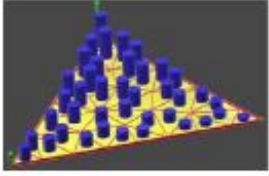
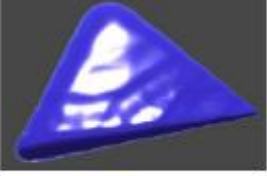
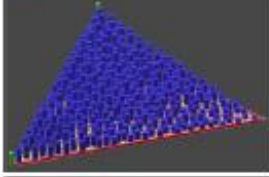
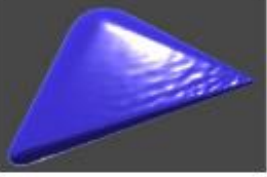
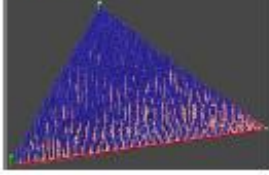
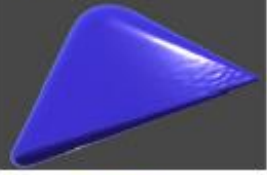
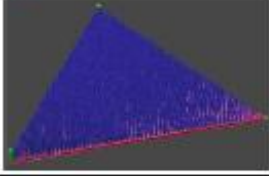
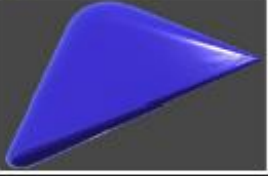
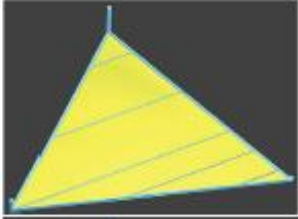
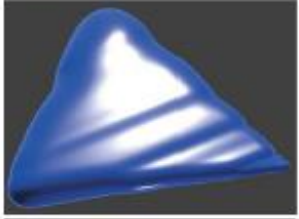
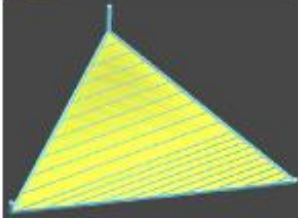
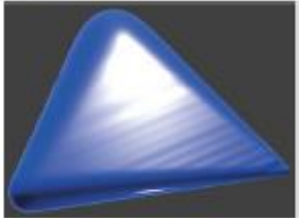
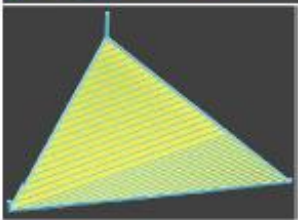
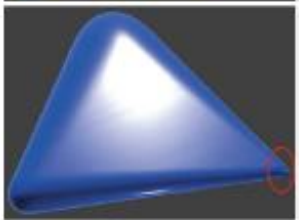
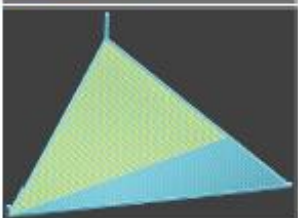
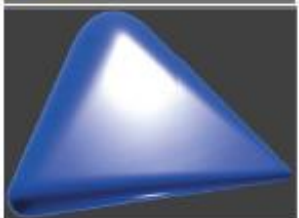
	Skeleton	Convolution surface	Sub-skeletons	Time(s)
(a)			1	15.590
(b)			1	4.480
(c)			4	16.743
(d)			40	159.951
(e)			319	1207.808
(f)			860	3182.045
(g)			3351	12644.94

Table 3
Semi-numerical integration [2,10] for a triangle skeleton with varying radii.

	Skeleton	Convolution surface	Sub-skeletons	Time(s)
(a)			6	33.277
(b)			20	113.272
(c)			40	229.347
(d)			100	601.513

As mentioned above, two different approaches of controlling varying thickness can be used for the unified polygon interpolation: field weight interpolation with unified support radius (Table 1(b)–(e)) and support radius interpolation (Table 1(f)–(i)). From Table 1, both methods are compared based on different polygons, and the results show that the latter one is superior especially at very thin parts (Table 1(b)–(c), (f)–(g)). The reason can be explained as follows: 1) It is not suitable to produce thin convolution surfaces with a large support radius as a large support radius absorbs small details for its large filtering radius; 2) A uniform large support radius is the only choice if thick parts have to be satisfied. On the other hand, more shrinkage emerges due to the large unified support radius (Table 1(b), (f)). Although it can be improved to some extent by offsetting the polygon to a larger outer polygon (Table 1(d), (h)), support radius interpolation behaves much better for thin surface approximation.

In previous applications, if a polygon skeleton-based convolution surface with varying thickness is needed, a commonly used strategy is to triangulate the polygon followed by a triangle-based convolution field calculation with respective independent support radii. As listed in Table 2, uniform support radii can only generate prism-like surfaces with equal thickness all over the polygon (Table 2(b)). Low resolution triangulation results in step artifacts (Table 2(c)–(e)), and higher resolutions can only alleviate the bumpiness to some extent (Table 2(f),

(g)), but the computation cost increases rapidly. Although the semi-numerical integration [2,10] (Table 3) could effectively reduce the convolution field computation by convolving parallel trapezoids instead of irregular smaller triangles, the subdivision density of their method depends on the thickness of the surfaces (Table 3(c)), and it is necessary to subdivide a general polygon into sub-triangles before a semi-numerical integration (Fig. 14(a)(b)). Different from these approaches, our method can produce the shapes with varying thickness more efficiently (Table 2(a)), and it can be conveniently utilized for producing multi-vertex polygonal skeleton-based convolution surfaces with varying thickness (Fig. 15). As the support radii vary at different projection positions in our method, it is identical to the SCALE-surface in essence for each queried spatial point.

Theoretically, designing variable kernels in space is also a good alternative to create polygon skeleton-based convolution surfaces with varying thickness. However, it is non-trivial to deduce a closed-form solutions, especially for a finite support kernel. Although an analytical solution for a triangle skeleton with an infinite variable kernel may exist [38], it cannot be applied to a general planar polygon directly. That is, the smoothness of the resulting surface depends on all the vertices of the polygon rather than a subset of them, which will result in similar seam artifacts in Figs. 9 and 10. On the other hand, our barycentric method can be easily applied to other kernels. In Fig. 16, the infinite Cauchy

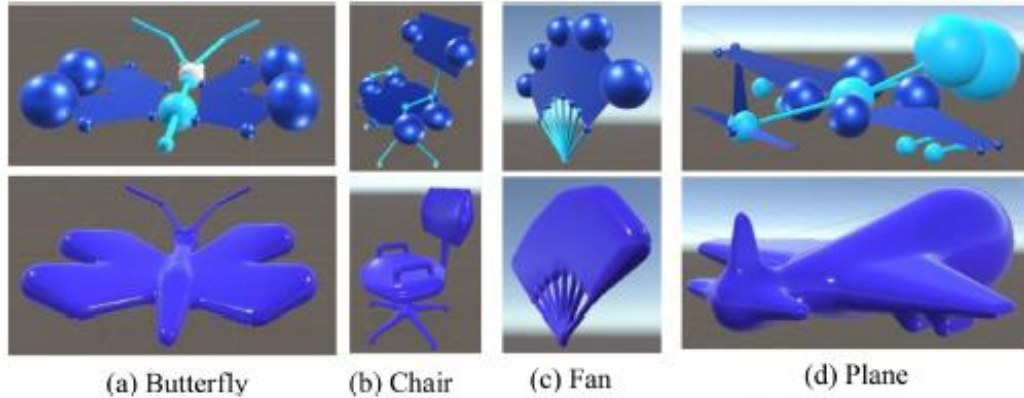


Fig. 15. Convolution surface approximation with our barycentric approach.

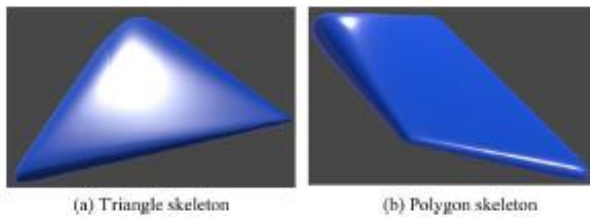


Fig. 16. Barycentric interpolation for Cauchy kernels.

kernel [38] is employed to create polygonal skeleton-based convolution surfaces with varying thickness by interpolating thickness and using a reasonable parameter λ .

Moreover, the barycentric method can also be adopted in other skeleton-based implicit surfaces, such as distance surfaces [40] (Fig. 17(b)). Although the intersection region is not as smooth as barycentric convolution surfaces (Fig. 17(d)), the result is better than the sub-triangle skeleton-based method (Fig. 17(c)).

7. Conclusion and future work

We have introduced a novel computation method of polygon skeleton-based convolution surfaces with varying radii using barycentric coordinates. Both field weight interpolation and support radius interpolation are addressed, and the latter one can produce much better approximations for thin skeleton vertices. The barycentric interpolation for a unified polygon is employed for its low computation cost and crease-free property. In addition, a winding number offset polygon with varying distance is adopted to compensate for convolution surface boundary shrinkage. Complex shapes with varying thickness can be easily created with our approach.

However, if the differences of a polygon's vertex radii are too distinct while the polygon is not big enough, it is still difficult to achieve an excellent approximation (Fig. 18). Moreover, the approximation error will increase when the skeleton becomes even smaller or when the difference of the radii at vertices becomes even larger. Additionally, the GPU acceleration can be further introduced for interactive practical applications.

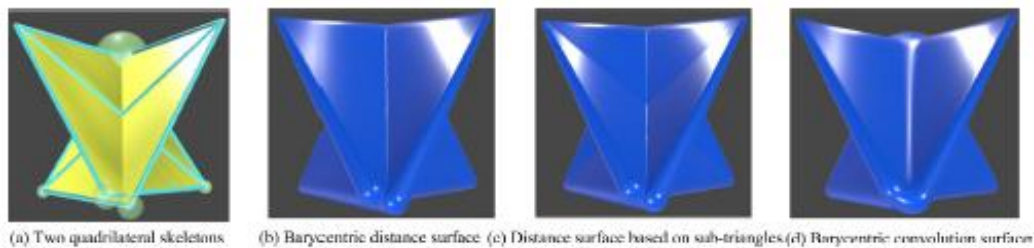


Fig. 17. Composed skeleton-based implicit surfaces.

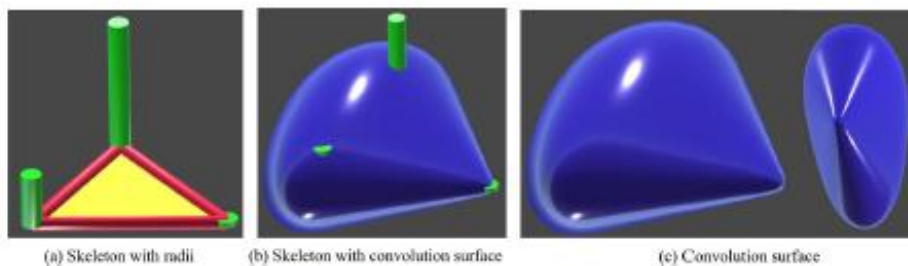


Fig. 18. A failure example.

Declaration of Competing Interest

The authors declare that they have no known competing financial interests or personal relationships that could have appeared to influence the work reported in this paper.

CRediT authorship contribution statement

Xiaoqiang Zhu: Conceptualization, Software, Writing - original draft. **Chenze Song:** Software, Methodology. **Mengyao Zhu:** Investigation, Methodology. **Xiangyang Wang:** Supervision. **Lihua You:** Writing - review & editing. **Xiaogang Jin:** Methodology, Writing - review & editing.

Acknowledgement

This work was supported by the National Natural Science Foundation of China (61831019, 61671011, 61801255) and Key Support Projects of Shanghai Science and Technology Committee (1601050100). Xiaoqiang Jin was supported by the Key Research and Development Program of Zhejiang Province (2018CD1090) and the Science and Technology Project on Preservation of Cultural Relics, Cultural Heritage Bureau of Zhejiang Province (Grant No. 2018009).

References

- [1] J.A. Barentzen, R. Abdrashitov, E. Singh, Interactive shape modeling using a skeleton-mesh co-representation, *ACM Trans. Graph.* 33 (4) (2014) 132:1–132:10.
- [2] C. Zanni, Skeleton-Based Implicit Modeling and Applications, Grenoble, 2013 Ph.D. thesis.
- [3] J. Bloomenthal, K. Shoemake, Convolution surfaces, in: Proceedings of the 18th Annual Conference on Computer Graphics and Interactive Techniques, SIGGRAPH 1991, 1991, pp. 251–256.
- [4] X. Jin, C.-L. Tai, Convolution surfaces for arcs and quadratic curves with a varying kernel, *Vis. Comput.* 18 (8) (2002) 530–546.
- [5] X. Zhu, X. Jin, S. Liu, H. Zhao, Analytical solutions for sketch-based convolution surface modeling on the GPU, *Vis. Comput.* 28 (11) (2012) 1115–1125.
- [6] X. Jin, C. Tai, J. Feng, Q. Peng, Convolution surfaces for line skeletons with polynomial weight distributions, *J. Graph. Tools* 6 (3) (2001) 17–28.
- [7] X. Jin, C.-L. Tai, Analytical methods for polynomial weighted convolution surfaces with various kernels, *Comput. Graph.* 26 (3) (2002) 437–447.
- [8] A.J.F. Suárez, E. Hubert, Convolution surfaces with varying radius: formulae for skeletons made of arcs of circles and line segments, *Res. Shape Anal.* (2018) 37–60.
- [9] X. Zhu, L. Song, L. You, M. Zhu, X. Wang, X. Jin, Brush2model: convolution surface-based brushes for 3d modelling in head-mounted display-based virtual environments, *Comput. Animat. Virtual Worlds* 28 (3–4) (2017) e1764.
- [10] C. Zanni, A. Bernhardt, M. Quillier, M. Cani, Scale-invariant integral surfaces, *Comput. Graph. Forum* 32 (8) (2013) 219–232.
- [11] E. Hubert, M. Cani, Convolution surfaces based on polygonal curve skeletons, *J. Symb. Comput.* 47 (6) (2012) 680–699.
- [12] A. Sherstyuk, Kernel functions in convolution surfaces: a comparative analysis, *Vis. Comput.* 15 (4) (1999) 171–182.
- [13] A. Bernhardt, A. Pihl, M.-P. Cani, I. Barthe, Matisse: painting 2d regions for modeling free-form shapes, in: EUROGRAPHICS Workshop on Sketch-Based Interfaces and Modeling, SBIM'08, Eurographics Association, Annecy, France, 2008, pp. 57–64.
- [14] S. Hornus, A. Angelidis, M. Cani, Implicit modeling using subdivision curves, *Vis. Comput.* 19 (2–3) (2003) 94–104.
- [15] X. Zhu, X. Jin, L. You, High-quality tree structures modelling using local convolution surface approximation, *Vis. Comput.* 31 (1) (2015) 69–82.
- [16] A.J.F. Suárez, E. Hubert, C. Zanni, Anisotropic convolution surfaces, *Comput. Graph.* 82 (2019) 106–116.
- [17] A.J. Puentes Suárez, Modeling Shapes with Skeletons: Scaffolds & Anisotropic Convolution, Université Côte D'Azur, 2019 Ph.D. thesis.
- [18] X. Jin, C.-L. Tai, H. Zhang, Implicit modeling from polygon soup using convolution, *Vis. Comput.* 25 (3) (2009) 279–288.
- [19] E. Hubert, Convolution surfaces based on polygons for infinite and compact support kernels, *Graph. Models* 74 (1) (2012) 1–13.
- [20] V. Gupta, P. Tandon, Heterogeneous object modeling with material convolution surfaces, *Comput.-Aided Des.* 62 (2015) 236–247.
- [21] A. Schmeißer, R. Wegener, D. Hirtel, H. Hagen, Smooth convolution-based distance functions, *Graph. Models* 82 (2015) 67–76.
- [22] Wadsworth, A Rational Finite Element Basis, Academic Press, New York, 1975.
- [23] P. Joshi, M. Meyer, T. DeRose, B. Green, T. Sanocki, Harmonic coordinates for character articulation, *ACM Trans. Graph.* 26 (3) (2007) 71.
- [24] M.S. Floater, Mean value coordinates, *Comput. Aided Geom. Des.* 20 (1) (2003) 19–27.
- [25] K. Hormann, M.S. Floater, Mean value coordinates for arbitrary planar polygons, *ACM Trans. Graph.* 25 (4) (2006) 1424–1441.
- [26] K. Hormann, N. Sukumar (Eds.), Generalized Barycentric Coordinates in Computer Graphics and Computational Mechanics, CRC Press, Boca Raton, FL, 2017.
- [27] Y. Lipman, D. Levin, D. Cohen-Or, Green coordinates, *ACM Trans. Graph.* 27 (3) (2008) 78:1–78:10.
- [28] Z. Li, D. Levin, Z. Deng, D. Liu, X. Luo, Cage-free local deformations using green coordinates, *Vis. Comput.* 26 (6–8) (2010) 1027–1036.
- [29] X. Li, S. Hu, Poisson coordinates, *IEEE Trans. Vis. Comput. Graph.* 19 (2) (2013) 344–352.
- [30] Y. Lipman, J. Kopf, D. Cohen-Or, D. Levin, GPU-assisted positive mean value coordinates for mesh deformations, in: Proceedings of the 18th Eurographics Symposium on Geometry Processing, Barcelona, Spain, July 4–6, 2007, 2007, pp. 117–123.
- [31] O. Weber, M. Ben-Chen, C. Gotman, Complex barycentric coordinates with applications to planar shape deformation, *Comput. Graph. Forum* 28 (2) (2009) 587–597.
- [32] T. Ju, Q. Zhou, M. van de Panne, D. Cohen-Or, U. Neumann, Reusable skinning templates using cage-based deformations, *ACM Trans. Graph.* 27 (5) (2008) 122:1–122:10.
- [33] J. Zhang, B. Deng, Z. Liu, G. Patané, S. Bouaziz, K. Hormann, L. Liu, Local barycentric coordinates, *ACM Trans. Graph.* 33 (6) (2014) 188:1–188:12.
- [34] D. Anisimov, C. Deng, K. Hormann, Subdividing barycentric coordinates, *Comput. Aided Geom. Des.* 43 (2016) 172–185.
- [35] D. Anisimov, D. Panozzo, K. Hormann, Blended barycentric coordinates, *Comput. Aided Geom. Des.* 52 (2017) 205–216.
- [36] X. Li, T. Ju, S. Hu, Cubic mean value coordinates, *ACM Trans. Graph.* 32 (4) (2013) 126:1–126:10.
- [37] R. Beaton, M.S. Floater, C.E. Klshagen, Hermite mean value interpolation on polygons, *Comput. Aided Geom. Des.* 60 (2018) 18–27.
- [38] J. McCormack, A. Sherstyuk, Creating and rendering convolution surfaces, *Comput. Graph. Forum* 17 (2) (1998) 113–120.
- [39] X. Chen, S. Memains, Polygon offsetting by computing winding numbers, in: IDETC/CIE 2005: ASME Int.Design Engineering Technical Conf. and Computers and Information in Engineering Conf., number DETC2005-85513 (Design Engineering Division and Computers and Information in Engineering Division, Long Beach, CA, 24/28 September 2005), 2005, pp. 565–575.
- [40] P. Shirley, S. Marschner, Fundamentals of Computer Graphics, 3rd ed., A. K. Peters, Ltd., Natick, MA, USA, 2009.